

5 Propagating Measurement Uncertainty into Nonlinear Behavioural Models

5.1 Introduction

The requirement of behavioural models for nonlinear microwave devices was introduced in Chapter 1 of this dissertation, where it was shown they can provide an intellectual-property-friendly “black-box” method to accurately predict device performance.

The core aim of a behavioural model is to fit mathematical functions to measurement data in order to reduce the amount of information stored within the extracted model (in contrast to a look-up table approach where the entire measurement dataset is indexed). This reduces both data storage requirements, making the model more portable, and also the computational requirements for accessing the model dataset when used in circuit simulators during design. Nonlinear behavioural models have developed over time and there are several different formulations in use today, of which the most common will be described in this Chapter. The reason there is no single “best” model is a question of application. Models which are most efficient and fit functions to more data dimensions may not be accurate for all device behaviours, whereas other models are more versatile but less data-efficient.

Before this project, no prior published work propagated a rigorous evaluation of measurement uncertainty through measurement data into an extracted nonlinear behavioural model. This information is of great use to both the modelling engineer, who can evaluate the sensitivities of their behavioural model to different sources of error in the measurement and extraction procedures, and the design engineer, who can quantify and compare the combined uncertainty in performance characteristics of circuits simulated using the extracted model. Both of these benefits will be presented in this Chapter.

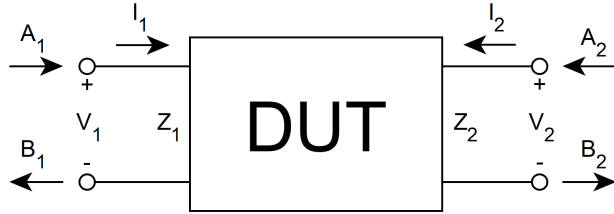


Figure 5.1: A representation of the different quantities described in nonlinear behavioural models, shown for a typical two-port device-under-test (DUT).

5.2 Nonlinear Behavioural Models

We shall first introduce a generic frequency-domain model of the nonlinear device, illustrated in Figure X, which defines the various quantities required to understand the following behavioural models. The power waves A and B at port n can be written as:

$$A_n = \frac{V_n + I_n Z_n}{2\sqrt{\Re(Z_n)}} \quad (5.1)$$

$$B_n = \frac{V_n - I_n Z_n^*}{2\sqrt{\Re(Z_n)}}, \quad (5.2)$$

where V and I are voltages and currents, respectively, and Z is the port impedance - typically 50-Ohms.

5.2.1 The Volterra “VIOMAP” Model

One of the first examples of a nonlinear behavioural model for microwave amplifiers was the Volterra input-output map, or “VIOMAP” [1]. This model was developed in the early nineties by Verbeyst and Vanden Bossche of the Hewlett Packard Network Measurement and Description Group (NMDG¹) at Vrije University in Brussels. In an effort to find an S-parameter equivalent for nonlinear devices, VIOMAP replaces the parameters themselves with a sum of Volterra kernel components at each harmonic frequency[2], [3].

Although the VIOMAP model was shown to be cascadable [1], applicable across the Smith chart for efficient load-pull measurements [4], and useful for characterising predistortion [5], it had two major shortcomings. Firstly, it could only be used to model weakly nonlinear devices.

¹now owned by National Instruments

This issue was tackled by introducing orthogonal polynomials on which to base the Volterra kernel [6], although the choice of these polynomials was not clear to users and required a lot of computation, thus they were not widely adopted. Secondly, the measurement procedure was customised to suit different applications, which appeared to increase the barrier for entry to new users who could not confidently buy standard equipment to perform the measurements.

5.2.2 Scattering Functions

Scattering functions, originally termed describing functions from their nonlinear analysis origin, were introduced by Verspecht and reduced the computational overhead for modelling strong nonlinearities when compared to the VIOMAP model [7]. They are expressed as a function mapping N complex numbers representing the input signal A into the k^{th} spectral component of the output signal B :

$$B_k = F_k(A_1, A_2, \dots, A_N), \quad (5.3)$$

where F_k is the scattering function for k . The VIOMAP model can be shown to be a subset of the scattering function approach, where the functions are constrained to a limited set of polynomials.

It should be mentioned here that all models described in this section require the device to be time-invariant, meaning that a time delay (or phase shift) in the input signal causes an equivalent time delay (or phase shift) in the output signal. This is typically the case for amplifiers, but more integrated communications components which include, for example, internal oscillators, cannot be modelled using the approaches described in this chapter.

Similar to the VIOMAP model, scattering functions are also complicated to apply and were not popular as a nonlinear modelling paradigm.

5.2.3 Hot S-parameters

Hot S-parameters were developed as a nonlinear behavioural model to extend S-parameters and allow stability and distortion characterisation of amplifiers [8], [9]. The model has several variations depending on the behaviour of interest, and there also exists an enhanced hot S-parameter model which incorporates additional information (in anticipation of the polyharmonic distortion model and the X-parameter model derived from it, which is described later).

Fundamentally, the hot S-parameter model, when used to characterise the distortion of amplifiers, provides a set of S-parameter measurements which are indexed against both frequency f (like standard S-parameters) and also the amplitude of the incident tone $|a_1|$:

$$\begin{bmatrix} B_1(f) \\ B_2(f) \end{bmatrix} = \begin{bmatrix} \text{hot}S_{11}(f, |A_1|) & \text{hot}S_{12}(f, |A_1|) \\ \text{hot}S_{21}(f, |A_1|) & \text{hot}S_{22}(f, |A_1|) \end{bmatrix} \begin{bmatrix} A_1(f) \\ A_2(f) \end{bmatrix} \quad (5.4)$$

The enhanced version of the model includes two additional parameters which describe more completely the nonlinear output matching characteristic ($\text{hot}S_{22}$):

$$\begin{bmatrix} B_1(f) \\ B_2(f) \end{bmatrix} = \begin{bmatrix} \text{hot}S_{11}(f, |A_1|) & \text{hot}S_{12}(f, |A_1|) \\ \text{hot}S_{21}(f, |A_1|) & \text{hot}S_{22}(f, |A_1|) \end{bmatrix} \begin{bmatrix} A_1(f) \\ A_2(f) \end{bmatrix} + \begin{bmatrix} T_{12}(f, |A_1|) \\ T_{22}(f, |A_1|) \end{bmatrix} e^{j\phi(A_1(f))} A_2^*(f) \quad (5.5)$$

where $e^{j\phi(a_1(f))}$ normalises the phase of a_2 relative to a_1 , a_2^* is the conjugate of a_2 and T_{ij} are the two new parameters in the enhanced model.

For an amplifier operating in the nonlinear regime, both the magnitude and phase of reflections at the output, due to matching, can have a significant impact on the device performance [10, Figure 12.13]. Figure 5.2 illustrates versions of the hot S-parameter model with different $\text{hot}S_{22}$ definitions.

The amplifier stability form of hot S-parameters will not be discussed here, but an overview is available in [9].

5.2.4 X-Parameters

X-parameters [11], from Keysight, are the commercial realisation of the poly-harmonic distortion model [12], which itself is an application of scattering functions with particular constraints. The most significant constraint is that any output of device which the model is applied to behaves linearly with respect to incident tones at harmonics of the fundamental, which is illustrated in Figure 5.3.

The X-parameter formulation can be developed from the scattering function origin. Firstly, the output $B_{p,k}$, at port p and harmonic k , is defined as:

$$B_{p,k} = \sum_{q,l} S_{p,k;q,l}(|A_{1,1}|) P^{k-l} A_{q,l} + \sum_{q,l} T_{p,k;q,l}(|A_{1,1}|) P^{k+l} A_{q,l}^*, \quad (5.6)$$

where $A_{q,l}$ is the input at port q and harmonic index l , and P is a phase normalisation coefficient such that $P = e^{j\phi(A_{1,1})}$, similar to (5.5). This equation contains two scattering

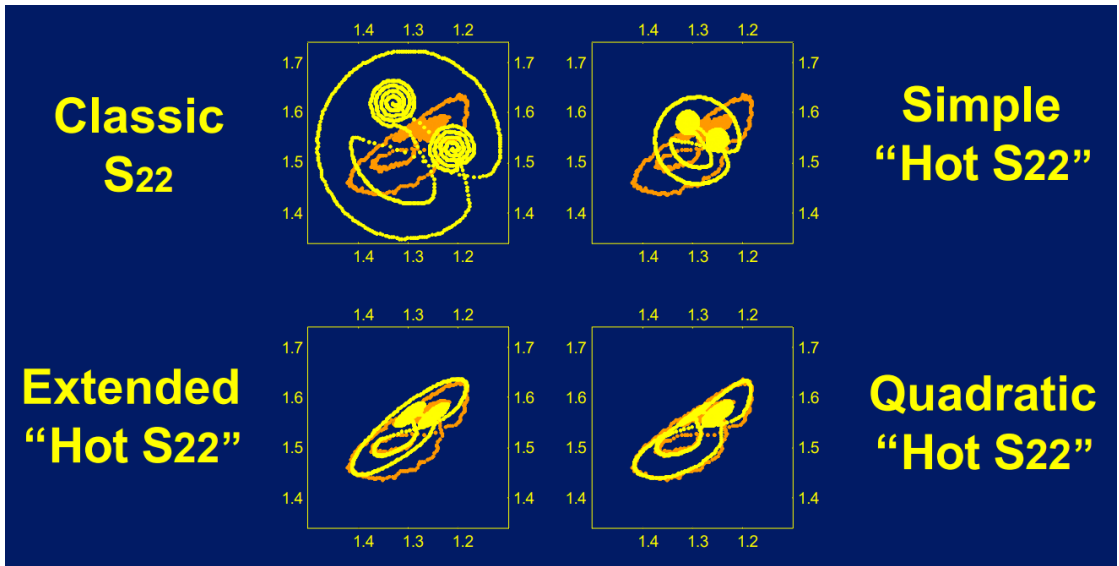


Figure 5.2: Performance of hot S-parameter models with different *hotS22* definitions, showing in polar form the measured (orange) and predicted (yellow) b_2 wave for a modulated large-signal a_1 wave, with values in Volts. Classic S_{22} means no dependence of S_{22} on $|a_1|$, simple “Hot S_{22} ” means a linear dependence of S_{22} on $|a_1|$, extended “Hot S_{22} ” includes dependence of S_{22} on $|a_1|$ and a_2 , and quadratic “Hot S_{22} ” includes a second order dependence of S_{22} on a_2 [8].

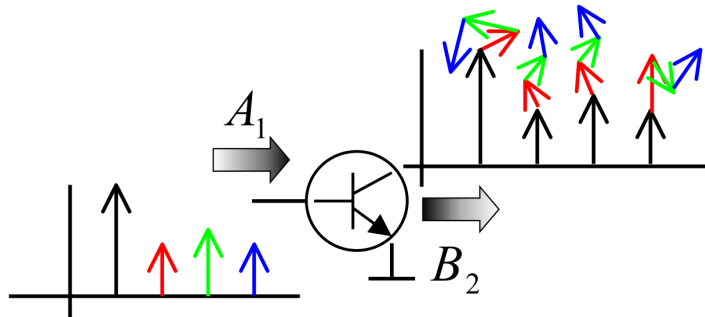


Figure 5.3: The harmonic superposition principle. If the input at port one (A_1) contains several small-signal harmonics, the output at port two (B_2) will comprise of the large-signal response plus the sum of responses due to each small-signal input harmonic, at each frequency [12]. The plots show complex phasors of increasing harmonic index along the horizontal axis, where the colour of the output phasors relate to the contribution from the respective input phasor.

functions which are sensitive to the large-signal input at the fundamental, $A_{1,1}$. The second function, $T_{p,k;q,l}$, is identical to $S_{p,k;q,l}$ except that it is a coefficient of the conjugate of the input wave, $A_{q,l}^*$. As with the enhanced Hot S-parameters, this is a more generalised way to incorporate the sensitivity of the model to the phase of input signals at harmonics on any port. Mathematically, the requirement of these two functions is a result of the non-analyticity of the complex-valued scattering functions. It is possible to instead define the functions in terms of real and imaginary components, but the normal and conjugate definition is standard for X-parameters and so will be taken forward here.

Because the phase is normalised with respect to that of $A_{1,1}$, we can also define $T_{p,k;1,1} = 0$ as the entire device response for this port and harmonic combination will be captured in $S_{p,k;1,1}$, which also represents the response to the large-signal input at port one at the fundamental tone. If we assume that the harmonic superposition principle is valid for our model, we can then simplify it by extracting the large-signal response as a separate term and treat the remaining functions as linear, with the restriction that they do not apply when $q,l = 1,1$. A good overview of this linearisation process of scattering functions is provided in [13].

We can now write our model as:

$$B_{p,k} = X_p^F(|A_{1,1}|)P^k + \sum_{q,l \neq (1,1)} [X_{p,k;q,l}^S(|A_{1,1}|)A_{q,l}P^{k-l} + X_{p,k;q,l}^T(|A_{1,1}|)A_{q,l}^*P^{k+l}], \quad (5.7)$$

where X^F (the large-signal term), X^S and X^T (the small-signal terms) are called X-parameters.

Two informative comparisons between the performance of scattering functions and X-parameters in modelling nonlinear device behaviour can be found in [14], [15].

The X-parameter model is heavily marketed by Keysight to be a complete solution for modelling nonlinear device behaviour. Additions to the model include mixer characterisation using multi-tone stimuli [16], the inclusion of memory effects [17], the prediction of load-pull performance from a single X-parameter measurement at 50-Ohms [18], and recently the inclusion of electro-thermal effects [19]. The X-parameters themselves are closely related to elements of the Jacobian matrix used within harmonic balance simulations. This feature means that X-parameters can be extracted in a straightforward way from circuit simulations, and existing X-parameter models based on measurements can be included in simulations. At least two circuit simulators support X-parameter models at the time of writing, including Keysight Advanced Design System (ADS) [20] and National Instruments AWR Microwave Office [21].

5.2.5 The Cardiff Model

Although X-parameters are sufficient to characterise the nonlinear behaviour of many amplifiers, the standard model² only includes third-order mixing products (via the $P^{(.)}$ terms in (5.7)). While the harmonic superposition principle holds, which is the case for weak-to-moderate nonlinear devices with well-matched ports, this is not always true for strongly nonlinear devices such as unpackaged transistors, amplifiers driven in class F modes, or devices with port impedances far from 50-Ohms. In order to avoid this X-parameters can be extracted as a function of both $|A_{1,1}|$ and $A_{2,1}$, but this can increase the model size significantly, especially for load-pull applications with phase and magnitude sweeps of $A_{2,1}$ [22]. An alternative approach, The Cardiff model, named after it's origin at Cardiff University, UK, incorporates n^{th} -order mixing products (typically truncated to seventh-order terms) and reduces the model dependence for fundamental load-pull to $|A_{1,1}|$ and $|A_{2,1}|$ only [23], [24].

The formulation of the Cardiff model is represented differently to that of X-parameters, however, they are a natural extension of that model and are equivalent when used with third-order mixing products. The measurement and extraction process is usually performed with a sampler-based NVNA featuring a real-time sampling oscilloscope and consists of a load-pull measurement [25].

For this project, X-parameters were chosen as the nonlinear behavioural model for which to focus on developing an uncertainty propagation, due to their current popularity. The framework which has been developed can be extended to include other models, but does not currently support them. Therefore, the Cardiff model will not be discussed in any greater detail here.

5.3 X-Parameter Extraction Procedure

X-parameters can be extracted from either measured or simulated data. A least-squares estimation can be used for both cases, however it is often more efficient to extract X-parameters directly from harmonic balance internal variables when simulating data. This section will describe the process involved for the least squares estimation of X-parameters from measured data, and two implementations developed during this project.

²It is possible to extend the X-parameter model to include higher order mixing products, however this is not supported by commercial measurement or simulation solutions.

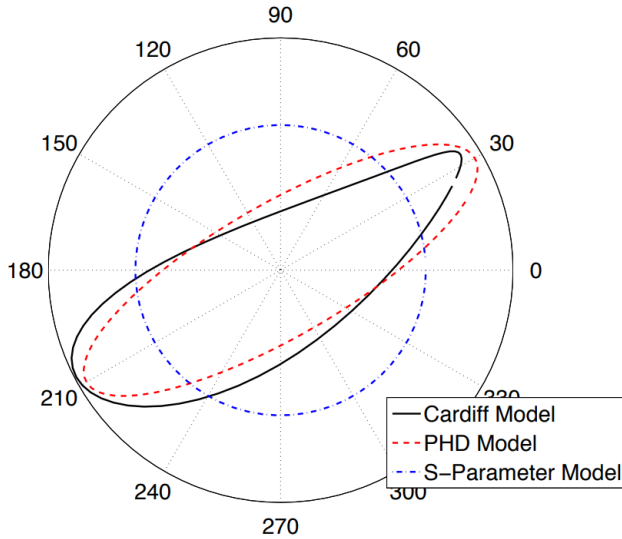


Figure 5.4: The relationship of device output $b_{p,k}$ against varying input wave phase $\angle a_{q,l}$ ($q, l \neq 1, 1$) for different nonlinear behavioural models, showing the effect that higher order mixing products have on the accuracy of the model [26].

5.3.1 Method

To perform device measurements from which X-parameters can be extracted, an NVNA setup as shown in Chapter 2 must be prepared, with the additional requirement of a second signal source which can be applied at either of two ports. All measurements taken during this project used the following Keysight equipment: an N5247A PNA-X NVNA, N1913A EPM Series Power Meter and two U9391G Comb Generators as phase references. Variables used in this section are in reference to (5.7).

The large-signal X-parameter, X_F , is simple to measure as it captures to the response of the device to a single large-signal drive tone at the fundamental frequency on port one ($A_{1,1}$). It is indexed against $|A_{1,1}|$, so this power is swept and measurements at each port p and harmonic k are made. The drive tone amplitude $|A_{1,1}|$ is said to define a large-signal operating point (LSOP) against which all of the X-parameters are indexed.

The small-signal X-parameters, X_S and X_T , model the interactions between small-signals incident to the device and $A_{1,1}$. To capture this behaviour, measurements are made with a second tone (“extraction” or “tickler” tone) applied to each port and harmonic in turn. If we ignore the conjugate term X-parameter X_T (which is similar to the simple “Hot S22” model in

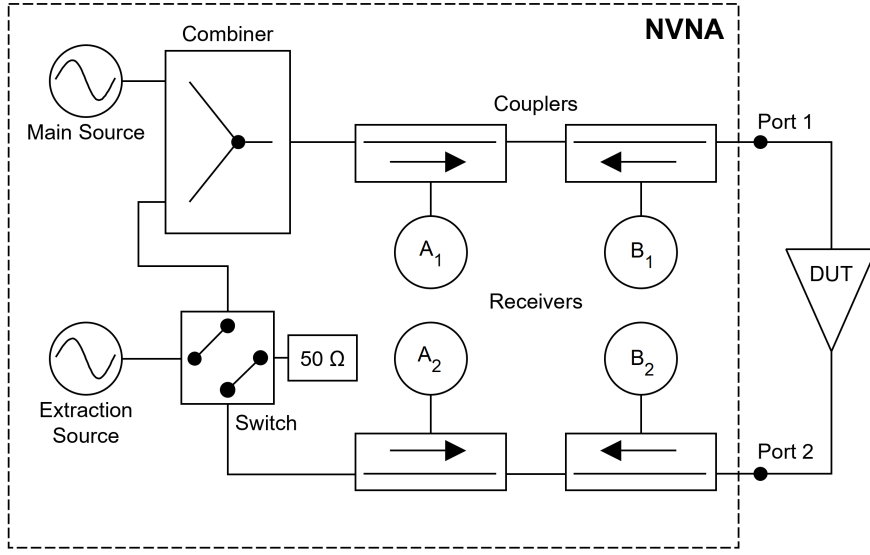


Figure 5.5: The NVNA setup required for X-parameter measurements. The switch terminates the unused port to a 50-Ohm load. The phase reference is connected to a spare receiver but not shown.

Figure 5.2), these measurements are all that is required to extract X-parameters. This equates to $N + N \times Q \times L$ stimulus conditions, where N is the number of LSOPs, Q is the number of ports and L is the number of harmonics. For each stimulus condition, the NVNA measures the device output on all ports at each harmonic. A diagram of the NVNA setup required for these measurements is shown in Figure 5.5.

However, to extract the full X-parameter model we must make additional measurements to characterise the phase-dependence of the mixing products between the extraction tones and the LSOP. This is the behaviour captured by the X_T parameters. Two measurement methods were developed to perform this task: offset-frequency and offset-phase. The offset-frequency method is not supported by the current version of the PNA-X firmware and appears to have fallen out of use, so the offset phase method alone will be explained. Further information can be found in [11].

Instead of a single extraction tone applied at each port and harmonic, a second measurement must be performed at an orthogonal phase ($\theta + 90^\circ$) to the initial extraction tone. An illustration of these measurements using phasors is given in Figure 5.6. After subtracting the large-signal only measurement from these two new measurements, we obtain two small-signal contributions which can be used to solve the following equations:

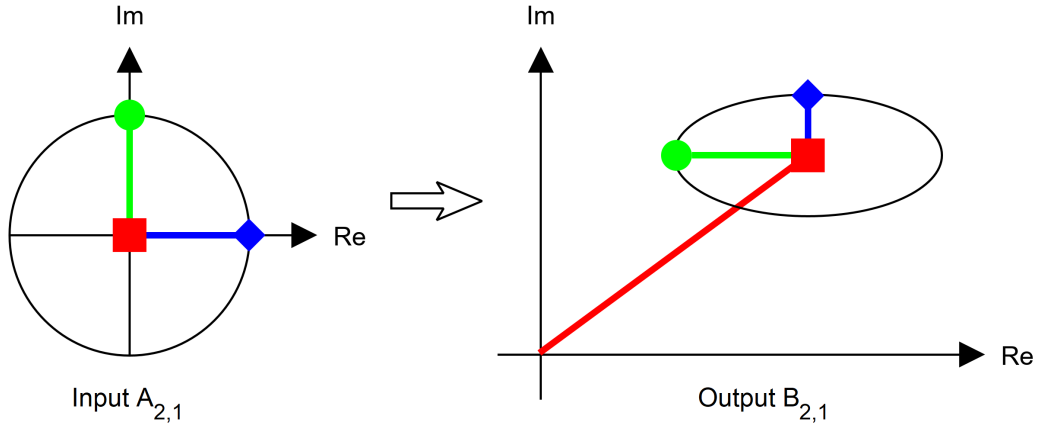


Figure 5.6: An example of the offset-phase method for measuring device response for X-parameter extraction. The red stimulus is with no extraction tone, and the blue and green stimuli are with extraction tones applied at 0° and 90°, respectively. Although $A_{2,1}$ and $B_{2,1}$ are specified, this effect occurs for all tones other than the fundamental on port one [12].

$$b_{p,k}^{SS1} = X_{p,k,q,l}^S a_{q,l}^{SS1} + X_{p,k,q,l}^T (a_{q,l}^{SS1})^*, \quad (5.8)$$

$$b_{p,k}^{SS2} = X_{p,k,q,l}^S a_{q,l}^{SS2} + X_{p,k,q,l}^T (a_{q,l}^{SS2})^*. \quad (5.9)$$

Of course, it is advised to make more than two measurements of different extraction tone phases (typically four) and solve for X_S and X_T using a least-squares estimation. The extraction process can in fact be simplified further by using a matrix least-squares arrangement to solve for the entire X-parameter model, which removes the need to subtract the large-signal response from all the extraction tone measurements. If we define a matrix X such that each row contains the NVNA measurements for a single extraction tone stimulus setting (of QL total):

$$X = \begin{bmatrix} 1 & a_{(2,1)_1} & a_{(2,1)_1}^* & a_{(1,2)_1} & a_{(1,2)_1}^* & a_{(2,2)_1} & a_{(2,2)_1}^* & \dots \\ 1 & a_{(2,1)_2} & a_{(2,1)_2}^* & a_{(1,2)_2} & a_{(1,2)_2}^* & a_{(2,2)_2} & a_{(2,2)_2}^* & \dots \\ \vdots & \dots \\ 1 & a_{(2,1)_{QL}} & a_{(2,1)_{QL}}^* & a_{(1,2)_{QL}} & a_{(1,2)_{QL}}^* & a_{(2,2)_{QL}} & a_{(2,2)_{QL}}^* & \dots \end{bmatrix} \quad (5.10)$$

and a vector y of length QL is defined to contain the respective measurements of a single output wave $b_{p,k}$:

$$y = \begin{bmatrix} b_{(p,k)_1} \\ b_{(p,k)_2} \\ \vdots \\ b_{(p,k)_{QL}} \end{bmatrix}, \quad (5.11)$$

then the X-parameters can be solved for using the following least-squares equation:

$$\beta = (X^\top X)^{-1} X^\top y \quad (5.12)$$

with the vector β containing the X-parameters:

$$\beta = \begin{bmatrix} X_{p,k}^F \\ X_{p,k,2,1}^S \\ X_{p,k,2,1}^T \\ X_{p,k,1,2}^S \\ X_{p,k,1,2}^T \\ X_{p,k,2,2}^S \\ X_{p,k,2,2}^T \\ \vdots \end{bmatrix}. \quad (5.13)$$

5.3.2 Implementation

5.3.2.1 PNA-X Extraction

5.3.2.2 MUF Custom Post-Processor

5.4 Evaluation of the Combined Standard Uncertainty of X-Parameters Extracted from Measurement Data

5.5 Propagation of Uncertainty from X-Parameters into Circuit Simulations

5.6 Design and Simulation using Nonlinear Behavioural Models Incorporating Measurement Uncertainty

The NIST MUF was used to perform the calibration of electromagnetic wave parameters measured using a Keysight Technologies 67 GHz N5247A PNA-X LSNA. The DUT was an internally matched Analog Devices HMC342LC4 low noise amplifier [27] mounted on a connectorised evaluation board. This amplifier has a typical gain of 19 dB and a 1-dB compression point at approximately 9 dBm output power at 25 GHz. To obtain results showing both the linear and nonlinear regimes of operation, the source power was swept between -22 dBm and -2 dBm in 0.25 dB steps. The fundamental frequency was set at 25 GHz, with a harmonic at 50 GHz also measured. The evaluation board used 2.92 mm precision connectors, connected via adapters to cables with 2.4 mm precision connectors. The calibration plane was located between the cables and the adapters (i.e. the adapters were included as part of the DUT), and the measurement setup had a nominal impedance of $50\text{-}\Omega$. The intermediate frequency bandwidth (IFBW) was set to 10 Hz. The built-in X-parameter measurement routine was used and configured to extract cross-frequency terms between both harmonics using measurements at 4 extraction tone phases (this is the default setting). A photograph of the setup is shown in Figure 5.7.

Uncertainties are propagated through all steps of the calibration by the MUF. We have included uncertainties present in the definitions and measurements of the passive calibration standards, the power meter calibration and measurement, the phase reference characterization and measurement, cable flexure, and connection repeatability of all calibration steps. Uncertainty

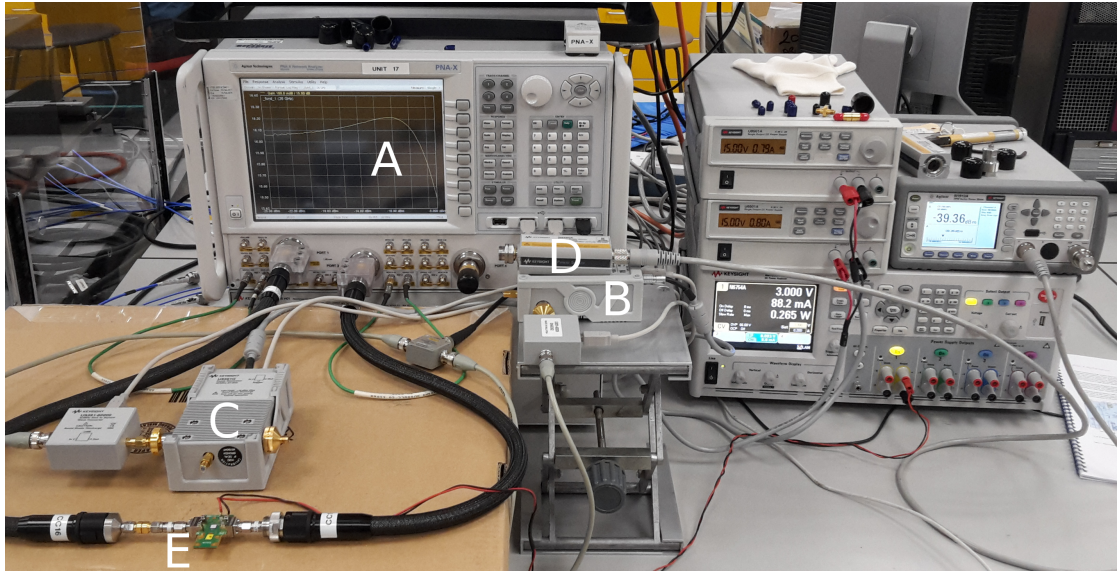


Figure 5.7: The measurement setup used for extracting X-parameters from the DUT. Shown is the PNA-X LSNA (A), the phase reference comb generator (B), the phase calibration comb generator (C), the power meter (D), and the connected DUT (E).

Table 5.1: Nominal values and standard uncertainties for the TRL coaxial line standards.

| Dimension | Line 1 value (mm) | Line 2 value (mm) |
|-------------------|--------------------|--------------------|
| Line length | 13.004 ± 0.003 | 14.913 ± 0.003 |
| Line inside dia. | 0.803 ± 0.001 | 0.803 ± 0.008 |
| Line outside dia. | 1.850 ± 0.005 | 1.850 ± 0.005 |

due to random noise in the high-dynamic range receivers was omitted as it has been shown to be negligible with respect to that arising from other error sources in LSNA measurements [28].

The MUF supports several calibration algorithms, and for this measurement the multiline TRL calibration algorithm [29], [30] was chosen to allow direct dimensional traceability to national measurement standards. The calibration standards used were from a 1.85 mm precision coaxial calibration kit (Rosenberger RPC-1.85 LRL). Table 5.1 gives the dimensions of the line standards used for the calibration. To include the effect of connector repeatability on the passive calibration, each standard was measured several times with the connector oriented differently. These measurements were passed to a MUF program (“Combine”) which produces a mean value with an associated uncertainty.

Table 5.2: Standard uncertainties for power meter uncertainty contributions derived in [31]

| Contribution | Standard uncertainty |
|--|-----------------------|
| Reference oscillator mismatch | 0.2% |
| Reference oscillator power uncertainty | 0.6% |
| Zero-set error | 0.5% meter full scale |
| Zero carry-over error | 0.2% meter full scale |
| Instrumentation error | 0.5% meter full scale |
| Calibration factor error | 0.024 |

Table 5.3: Nominal phase and standard uncertainty for harmonic phase reference at calibration frequencies

| Frequency (GHz) | Characterized phase (deg.) | Measured phase (deg.) |
|-----------------|----------------------------|-----------------------|
| 25 | 181.5 ± 0.4 | -16.8 ± 1.5 |
| 50 | 170.8 ± 1.0 | 61.0 ± 2.5 |

The power meter measurement, as part of the absolute calibration, measures the amplitude of the waves. The calibration model for the power meter itself is defined in [31] and includes the reference oscillator mismatch, the reference oscillator power uncertainty, the zero-set error, the zero carry-over error, the instrumentation error, and error in the power sensor calibration factor. The estimates and uncertainties used for these parameters in the calibration are shown in Table 5.2 and are derived from specifications supplied by the manufacturer. The mismatch of the power sensor was also measured using a calibrated VNA and included in the absolute calibration. Connector repeatability was assessed for this measurement in the same way as for the passive standards.

In order to complete the absolute calibration, the phase must also be calibrated. This is performed using a harmonic phase reference, which for this calibration was provided by a Keysight Technologies 67 GHz comb generator[32]. This device supplies a stable and repeatable train of pulses, which creates a frequency comb (aligned to the calibration frequencies) to be measured by the LSNA. The phase uncertainties are given in Table 5.3 and were obtained through characterization with a sampling oscilloscope at NIST, which is traceable to national measurement standards via electro-optic calibration [33], [34].

5.6.1 X-Parameter Uncertainties

In this example we used Monte Carlo with 1000 samples to propagate uncertainty to the X-parameters of the DUT. This required 8 hours of processing for the calibration and a further 8 hours of processing for the X-parameter extraction. A histogram is provided in Figure 5.8 showing good agreement between the Monte Carlo and sensitivity analysis. This level of agreement is typical for all of the extracted X-parameters.

The estimated values and standard uncertainties from the Monte Carlo analysis for the magnitude and phase of a sample of X-parameter terms are shown in Figure 5.9. It can be seen in all plots that there is a clear change in uncertainty for several X-parameters as the DUT transitions between the linear and nonlinear regimes.

The phase noise seen at lower powers in the estimate of $X_{2,1;2,2}^T$ is not accompanied by an increase in measurement uncertainty. This suggests that it arises from the extraction routine, which contributes another source of uncertainty not studied in this paper. By design, the X^T parameters are negligible in the linear regime, and so this effect will have little contribution when the model is used.

5.7 Conclusions

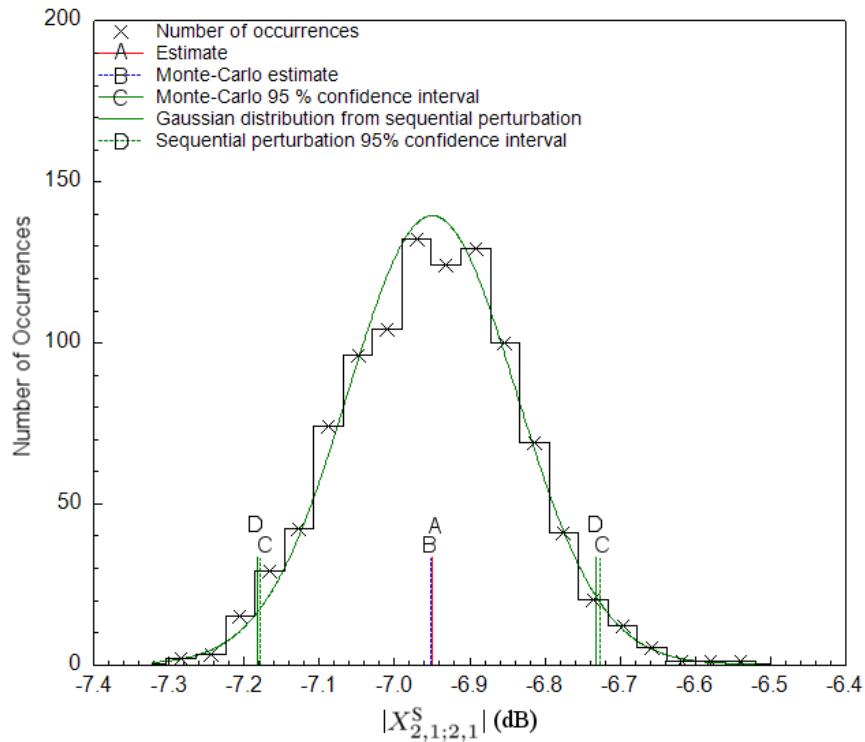


Figure 5.8: Histogram comparing the Monte Carlo and sequential perturbation uncertainty results for $X_{2,1;2,1}^S$ (25 GHz) of the DUT at -2.4 dBm source power. The vertical line in the center of the plot (A) shows the nominal value (estimate), (B) shows the Monte Carlo average, and (C, D) show the Monte Carlo and sequential perturbation 95% confidence intervals, respectively.

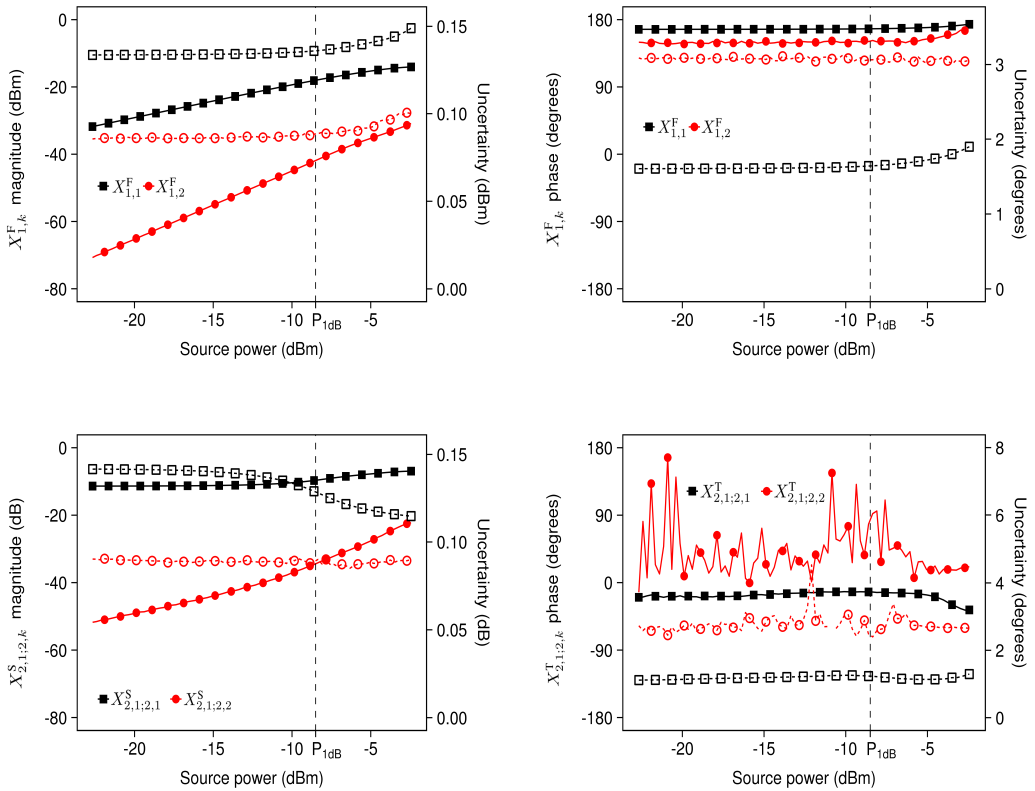


Figure 5.9: Estimates (solid line and shapes, left scale) and standard uncertainties (dashed line and hollow shapes, right scale) for the magnitude and phase of a sample of the extracted X-parameters. Harmonic indices 1 and 2 relate to measurement frequencies of 25 and 50 GHz, respectively. Uncertainties are a linear variation of the scale value.

References

- [1] F. Verbeyst and V. Bossche, “Viomap, the s-parameter equivalent for weakly nonlinear rf and microwave devices,” *IEEE Transactions on Microwave Theory and Techniques*, vol. 42, no. 12, pp. 2531–2535, Dec. 1994, ISSN: 0018-9480. DOI: [10.1109/22.339793](https://doi.org/10.1109/22.339793).
- [2] M. Schetzen, *The Volterra and Wiener Theories of Nonlinear Systems*. Melbourne, FL, USA: Krieger Publishing Co., Inc., 2006, ISBN: 1575242834.
- [3] H. Moodi and D. Bustan, “On identification of nonlinear systems using volterra kernels expansion on laguerre and wavelet function,” in *2010 Chinese Control and Decision Conference*, May 2010, pp. 1141–1145. DOI: [10.1109/CCDC.2010.5498146](https://doi.org/10.1109/CCDC.2010.5498146).
- [4] F. Verbeyst and M. Vanden Bossche, “The volterra input-output map of a high-frequency amplifier as a practical alternative to load-pull measurements,” *IEEE Transactions on Instrumentation and Measurement*, vol. 44, no. 3, pp. 662–665, Jun. 1995, ISSN: 0018-9456. DOI: [10.1109/19.387303](https://doi.org/10.1109/19.387303).
- [5] F. Verbeyst and M. V. Bossche, “Viomap, 16qam and spectral regrowth: Enhanced prediction and predistortion based on two-tone black-box model extraction,” in *45th ARFTG Conference Digest*, vol. 27, May 1995, pp. 19–28. DOI: [10.1109/ARFTG.1995.327101](https://doi.org/10.1109/ARFTG.1995.327101).
- [6] F. Verbeyst, “Using orthogonal polynomials as alternative for viomap to model hardly nonlinear devices,” in *47th ARFTG Conference Digest*, vol. 29, Jun. 1996, pp. 112–120. DOI: [10.1109/ARFTG.1996.327171](https://doi.org/10.1109/ARFTG.1996.327171).
- [7] J. Verspecht, D. Schreurs, A. Barel, and B. Nauwelaers, “Black box modelling of hard nonlinear behavior in the frequency domain,” in *1996 IEEE MTT-S International Microwave Symposium Digest*, vol. 3, Jun. 1996, 1735–1738 vol.3. DOI: [10.1109/MWSYM.1996.512277](https://doi.org/10.1109/MWSYM.1996.512277).
- [8] J. Verspecht, “Everything you’ve always wanted to know about hot-s22 (but we’re afraid to ask),” in *IEEE MIT-S Int. Microwave Symp. Worshop, paper no 95*, 2002.

- [9] J. Verspecht, D. Barataud, J. Teyssier, and J. Nébus, "Hot s-parameter techniques: $6 = 4 + 2$," in *2005 66th ARFTG Microwave Measurement Conference (ARFTG)*, Dec. 2005, pp. 1–9. DOI: [10.1109/ARFTG.2005.8373119](https://doi.org/10.1109/ARFTG.2005.8373119).
- [10] S. C. Cripps, *RF Power Amplifiers for Wireless Communications, Second Edition (Artech House Microwave Library (Hardcover))*. Norwood, MA, USA: Artech House, Inc., 2006, ISBN: 1596930187.
- [11] D. E. Root, J. Verspecht, J. Horn, and M. Marcu, *X-Parameters: Characterization, Modeling, and Design of Nonlinear RF and Microwave Components*, ser. The Cambridge RF and Microwave Engineering Series. Cambridge University Press, 2013. DOI: [10.1017/CBO9781139042970](https://doi.org/10.1017/CBO9781139042970).
- [12] Verspecht and D. E. Root, "Polyharmonic distortion modeling," *IEEE Microwave Magazine*, vol. 7, no. 3, pp. 44–57, Jun. 2006, ISSN: 1527-3342. DOI: [10.1109/MMW.2006.1638289](https://doi.org/10.1109/MMW.2006.1638289).
- [13] J. Verspecht, D. F. Williams, D. Schreurs, K. A. Remley, and M. D. McKinley, "Linearization of large-signal scattering functions," *IEEE Transactions on Microwave Theory and Techniques*, vol. 53, no. 4, pp. 1369–1376, Apr. 2005, ISSN: 0018-9480. DOI: [10.1109/TMTT.2005.845771](https://doi.org/10.1109/TMTT.2005.845771).
- [14] G. Sun, Y. Xu, and A. Liang, "The study of nonlinear scattering functions and x-parameters," in *2010 International Conference on Microwave and Millimeter Wave Technology*, May 2010, pp. 1086–1089. DOI: [10.1109/ICMMT.2010.5525111](https://doi.org/10.1109/ICMMT.2010.5525111).
- [15] C. Widemann, H. Weber, S. Schatz, and W. Mathis, "A comparison of the volterra series-based nonlinear s-parameters and x-parameters," in *2015 22nd International Conference Mixed Design of Integrated Circuits Systems (MIXDES)*, Jun. 2015, pp. 453–457. DOI: [10.1109/MIXDES.2015.7208562](https://doi.org/10.1109/MIXDES.2015.7208562).
- [16] C. Xie, T. Zhang, and D. Liu, "Using x-parameters to model mixers," in *2012 International Conference on Microwave and Millimeter Wave Technology (ICMMT)*, vol. 3, May 2012, pp. 1–3. DOI: [10.1109/ICMMT.2012.6230227](https://doi.org/10.1109/ICMMT.2012.6230227).
- [17] J. Verspecht, J. Horn, L. Betts, D. Gunyan, R. Pollard, C. Gillease, and D. E. Root, "Extension of x-parameters to include long-term dynamic memory effects," in *2009 IEEE MTT-S International Microwave Symposium Digest*, Jun. 2009, pp. 741–744. DOI: [10.1109/MWSYM.2009.5165803](https://doi.org/10.1109/MWSYM.2009.5165803).

- [18] D. E. Root, J. Verspecht, and J. Xu, “Closed-form solutions to large-signal pa problems: Wirtinger calculus applied to x-parameter,” in *2017 12th European Microwave Integrated Circuits Conference (EuMIC)*, Oct. 2017, pp. 212–215. DOI: 10.23919/EuMIC.2017.8230697.
- [19] S. J. Gillespie, D. E. Root, M. Marcu, and P. H. Aaen, “Electrothermal x-parameters for dynamic modeling of rf and microwave power transistors,” in *2018 13th European Microwave Integrated Circuits Conference (EuMIC)*, Sep. 2018, pp. 353–356. DOI: 10.23919/EuMIC.2018.8539893.
- [20] N. AWR. Microwave office, [Online]. Available: <https://www.awr.com/software/products/microwave-office> (visited on 08/16/2019).
- [21] K. Technologies. Advanced design system (ADS), [Online]. Available: <https://www.awr.com/software/products/microwave-office> (visited on 08/16/2019).
- [22] D. Gunyan, J. Horn, J. Xu, and D. E. Root, “Nonlinear validation of arbitrary load x-parameter and measurement-based device models,” in *2009 73rd ARFTG Microwave Measurement Conference*, Jun. 2009, pp. 1–4. DOI: 10.1109/ARFTG.2009.5278063.
- [23] S. Woodington, T. Williams, H. Qi, D. Williams, L. Pattison, A. Patterson, J. Lees, J. Benedikt, and P. J. Tasker, “A novel measurement based method enabling rapid extraction of a rf waveform look-up table based behavioral model,” in *2008 IEEE MTT-S International Microwave Symposium Digest*, Jun. 2008, pp. 1453–1456. DOI: 10.1109/MWSYM.2008.4633053.
- [24] H. Qi, J. Benedikt, and P. J. Tasker, “Nonlinear data utilization: From direct data lookup to behavioral modeling,” *IEEE Transactions on Microwave Theory and Techniques*, vol. 57, no. 6, pp. 1425–1432, Jun. 2009, ISSN: 0018-9480. DOI: 10.1109/TMTT.2009.2019996.
- [25] S. Woodington, R. Saini, D. Williams, J. Lees, J. Benedikt, and P. J. Tasker, “Behavioral model analysis of active harmonic load-pull measurements,” in *2010 IEEE MTT-S International Microwave Symposium*, May 2010, pp. 1688–1691. DOI: 10.1109/MWSYM.2010.5517261.
- [26] D. Bespalko, “Modular nonlinear characterization system and large-signal behavioral modelling of unmatched transistors for streamlined power amplifier design,” PhD thesis, University of Waterloo, Jan. 2016. [Online]. Available: <http://hdl.handle.net/10012/10179>.

- [27] *HMC342LC4 datasheet*, Analog Devices. [Online]. Available: <http://www.analog.com/media/en/technical-documentation/data-sheets/hmc342.pdf>.
- [28] P. S. Blockley, J. B. Scott, D. Gunyan, and A. E. Parker, “The random component of mixer-based nonlinear vector network analyzer measurement uncertainty,” *IEEE Transactions on Microwave Theory and Techniques*, vol. 55, no. 10, pp. 2231–2239, Oct. 2007, ISSN: 0018-9480. DOI: 10.1109/TMTT.2007.906515.
- [29] G. F. Engen and C. a. Hoer, ““Thru-Reflect-Line” : An improved technique for calibrating the dual six-port automatic network analyzer,” *IEEE Trans. Microw. Theory Techn.*, vol. 27, no. 12, pp. 987–993, Dec. 1979.
- [30] R. B. Marks, “A multiline method of network analyzer calibration,” *IEEE Trans. Microw. Theory Techn.*, vol. 39, no. 7, pp. 1205–1215, Jul. 1991, ISSN: 0018-9480. DOI: 10.1109/22.85388.
- [31] Keysight Technologies, “Fundamentals of RF and Microwave Power Measurements (Part 3),” Tech. Rep. 5989-7619EN, Sep. 2017.
- [32] ——, “U9391C/F/G Comb Generators,” Tech. Rep. 5988-9215EN, Aug. 2014.
- [33] H. C. Reader, D. F. Williams, P. D. Hale, and T. S. Clement, “Comb-generator characterization,” *IEEE Transactions on Microwave Theory and Techniques*, vol. 56, no. 2, pp. 515–521, Feb. 2008, ISSN: 0018-9480. DOI: 10.1109/TMTT.2007.914630.
- [34] P. D. Hale, A. Dienstfrey, J. C. M. Wang, D. F. Williams, A. Lewandowski, D. A. Keenan, and T. S. Clement, “Traceable waveform calibration with a covariance-based uncertainty analysis,” *IEEE Transactions on Instrumentation and Measurement*, vol. 58, no. 10, pp. 3554–3568, Oct. 2009, ISSN: 0018-9456. DOI: 10.1109/TIM.2009.2018012.